Asian Journal of Chemistry; Vol. 33, No. 11 (2021), 2715-2722

ASIAN JOURNAL OF CHEMISTRY

https://doi.org/10.14233/ajchem.2021.23147

FT-IR, FT-Raman, NMR Spectroscopic and DFT Quantum Chemical Investigations of 6-Methylcoumarin

R. KANIMOZHI[1] and V. ARJUNAN[2,3,*]

[1]Centre for Research and Evaluation, Bharathiar University, Coimbatore-641046, India
[2]Department of Chemistry, Kanchi Mamunivar Centre for Post-Graduate Studies, Puducherry-605008, India
[3]Department of Chemistry, Rajiv Gandhi Arts & Science College, Thavalakuppam, Puducherry-605007, India

*Corresponding author: E-mail: varjunftir@yahoo.com

Received: 22 June 2021; *Accepted*: 8 August 2021; *Published online*: 20 October 2021; AJC-20554

The structural geometry, electronic and reactivity characteristics, vibrational assignments and the fundamental modes of 6-methylcoumarin have been carried out. The effect of methyl group on the pyrone skeletal vibrations was also discussed. The experimental vibrational frequencies were compared with the wavenumbers obtained theoretically from the B3LYP method employing the high level 6-311++G** and cc-pVTZ basis sets. Frontier molecular orbital (FMO) energy and the LUMO-HOMO energy gap was measured. The atomic charges and the bond properties were examined by natural bond orbital analysis. The hydrogen and carbon environment were examined by NMR spectra. The nuclophilic, electrophilic and free radical attacking sites of 6-methylcoumarin were also analyzed.

Keywords: Methylcoumarin, FT-Raman, NMR, DFT, Reactivity descriptors.

INTRODUCTION

In medicinal and organic chemistry, coumarins and their derivatives play a critical role because of their structural variability and versatile synthetic methodologies [1-3]. In many species of bacteria, plants and fungi, numerous natural derivatives of coumarins are found [4,5]. Literature has reported their application as precursors or active products in pharmacology for new, effective pharmaceuticals and their biological properties. Moreover, coumarins act as photoreactive chromophores, which undergo reversible [2π + 2π] cycloaddition in the UV-Vis-NIR region after irradiation with specific wavelengths [8].

Studies on 3-acetylcoumarin [9] and 4-hydroxy-1-thiocoumarin [10], the structural changes of 7-hydroxy-4-methylcoumarin dimer [11], spectroscopic and quantum chemical electronic structure investigations of 3,4-dihydrocoumarin and 3-methylcoumarin [12], FT-IR, FT-Raman and UV-vis spectra and DFT calculations of 3-cyano-4-methylcoumarin [13], vibrational spectra, normal modes, *ab initio* and DFT calculations of 6-chloro- and 7-chloro-4-bromomethylcoumarin [14], vibrational and *ab initio* studies of 3-acetyl-6-bromocoumarin and 3-acetyl-6-methylcoumarin [15], density functional theory investigations and vibrational spectra of 7-acetoxy-6-(2,3-dibromopropyl)-4,8-dimethylcoumarin [16], theoretical study on 3-acetyl-6-bromocoumarin [17], infrared study of 6-methylcoumarin in binary solvent mixtures [18], FTIR and Raman spectral assignments for 6-methyl-4-bromomethyl-coumarin [19], inhibitory effects and oxidation of 6-methyl-coumarin, 7-methylcoumarin and 7-formylcoumarin *via* human CYP2A6 and its mouse and pig orthologous enzymes [20], biodistribution study of free and microencapsulated 6-methyl-coumarin [21], synthesis and evaluation of 6-methylcoumarin derivatives as potent and selective monoamine oxidase B inhibitors [22], antioxidant properties of hydroxy-3-arylcoumarins [23], photodimerization of 6-methylcoumarin [24], determination of 6-methylcoumarin and 7-methoxycoumarin in cosmetics [25] have also been reported.

To the best of our knowledge, no detailed structural, spectroscopic and reactivity studies have been undertaken on 6-methylcoumarin and owing to the vast biological applications of 6-methylcoumarin and derivatives of coumarin in an enormous field, an extensive structural, spectroscopic and quantum

chemical studies on 6-methylcoumarin have been carried out by using FT-IR, FT-Raman, FT-NMR spectroscopic techniques along with DFT studies for the first time in order to provide the structure characteristics, vibrations, reactivity properties and the effect of methyl group on the pyrone moiety.

EXPERIMENTAL

6-Methylcoumarin (6MC) was purchased from Sigma-Aldrich, USA and used as such without any purification. The FT-IR spectrum of the compound was recorded in liquid phase by CsI windows in a Bruker IFS66V spectrometer equipped with a Globar source, Ge/KBr beam splitter and a deuterated triglycine sulphide (DTGS) detector in the range of 4000-400 cm^{-1} with the spectral resolution of 2 cm^{-1}. The FT-Raman spectrum of the compound was also recorded with the same instrument with FRA 106 Raman module. The Raman spectrum was obtained in the wavenumber range 4000-100 cm^{-1}. The light scattering was excited using a low-noise diode pumped Nd:YAG laser source operating at 1.064 mm with 200 mW power. A special (enhanced) liquid nitrogen cooled germanium detector was used. The frequencies of all sharp bands are accurate to 2 cm^{-1}. The ^1H (400 MHz, DMSO) and ^{13}C (100 MHz, DMSO) NMR spectra were recorded on a Bruker HC400 instrument.

The structural parameters of 6-methylcoumarin (6MC) were determined with precision using the standard high level 6-311++G** and triple zeta cc-pVTZ basis sets incorporating both diffuse and polarization functions. Thus, the gradient corrected density functional theory (DFT) [26] with the three-parameter hybrid functional Becke3 [27,28] for the exchange part and the Lee-Yang-Parr (LYP) correlation functional [29], calculations have been carried out in the present investigation with Gaussian 09 [30] program. The harmonic vibrational frequency calculations were carried out resulting in IR and Raman frequencies together with intensities and Raman depolarization ratios. The dipole moment and polarizability tensors were computed analytically.

Isoelectronic molecular electrostatic potential surface (MEP) and electron density surface [31] were calculated using cc-pVTZ basis set. The molecular electrostatic potential (MEP) at a point 'r' in the space around a molecule (in atomic units) can be expressed as:

$$V(r) = \sum_A \frac{Z_A}{\left|\vec{R}_A - \vec{r}\right|} - \int \frac{\rho(\vec{r}')\,dr'}{\left|\vec{r}' - \vec{r}\right|}$$

where, Z_A is the charge on nucleus A, located at R_A and $\rho(r')$ is the electronic density function for the molecule. The first and second terms represent the contributions to the potential due to nuclei and electrons, respectively. V(r) is the resultant electric potential at each point 'r', which is the net electrostatic effect produced at the point 'r' by both the electrons and nuclei of the molecule. The electron density surface mapped with electrostatic potential depict the shape, size, charge density distribution and the site of chemical reactivity of a molecule. GaussView 5.0.8 visualization program [32] has been utilized to construct the MEP surface, electrostatic potential surface and the shapes of Frontier molecular orbitals.

The stabilization energy $E^{(2)}$ associated with the delocalization of i (donor) → j (acceptor) is estimated from the second-order perturbation method [33-35] as shown below:

$$E^{(2)} = q_i \frac{F^2(i,j)}{\varepsilon_j - \varepsilon_i}$$

where q_i is the donor orbital occupancy, β_i and β_j are diagonal elements (orbital energies) and F(i,j) is the off-diagonal Fock matrix element.

The ^1H and ^{13}C NMR isotropic shielding constants are calculated by GIAO method [36,37] using B3LYP/cc-pVTZ method. The effect of solvent is included using the PCM model. The chemical shifts (δ) with respect to tetramethylsilane (TMS) have been determined from the isotropic shielding constant values using the relation $\delta_{iso}(X) = \sigma_{TMS}(X) - \sigma_{iso}(X)$, where δ_{iso} = isotropic chemical shift and σ_{iso} = isotropic shielding constant.

The global and local descriptors of reactivity are determined utilizing finite difference approximation. Using the finite difference approximation, the Fukui functions for studying the reactivity at the atomic level are defined as:

$$f_k^+(r) = q_k(N+1) - q_k(N) \quad \text{for nucleophilic attack}$$

$$f_k^-(r) = q_k(N) - q_k(N-1) \quad \text{for electrophilic attack}$$

$$f_k^+(r) = \frac{1}{2}\left(q_k(N+1) - q_k(N-1)\right) \quad \text{for free radical attack}$$

The term q_k is the atomic charge of the k^{th} atom in the neutral (N), anion (N+1) or cation (N-1) molecular species. The local reactivity descriptors of the particular atom of the molecule ($s_k^a = f_k^a S, \omega_k^a = \omega f_k^a$ and f_k^a where a = +, - and 0) describing nucleophilic, electrophilic and free radical attack, respectively were also evaluated. The calculation of global electrophilicity is based on the equation $\omega = \mu^2/2\eta$. The multiphilicity descriptors ($\Delta\omega_k$), which can be simultaneously characterises a chemical species nucleophilic as well as electrophilic nature. If $(\Delta\omega_k) > 0$, then the site *k* is favoured for a nucleophilic attack, whereas if $(\Delta\omega_k) < 0$, then the site *k* may be favoured for an electrophilic attack.

RESULTS AND DISCUSSION

Structural properties: The optimized stable geometry of 6-methylcoumarin (6MC) with numbering of atoms is shown in Fig. 1. The optimized structural parameters namely bond lengths and bond angles of 6MC determined at B3LYP with 6-311++G** and cc-pVTZ basis sets are presented in Table-1 and compared with experimental data of 4-(4-chloroanilinomethyl)-6-methyl coumarin reported by Kokila *et al.* [38]. The data obtained by B3LYP/cc-pVTZ method is only taken for comparison unless otherwise stated. The actual C-O bond length in a six membered heterocyclic ring is 1.43 Å, but a significant reduction of O1-C10 bond length (1.36 Å) and O1-C2 (1.39 Å) is observed in present investigation is due to the fusion of benzene ring with α-pyrone ring. The variation of bond distances between O1-C2 and O1-C10 in coumarin derivatives is a quite common feature and confirmed in the present investigation also.

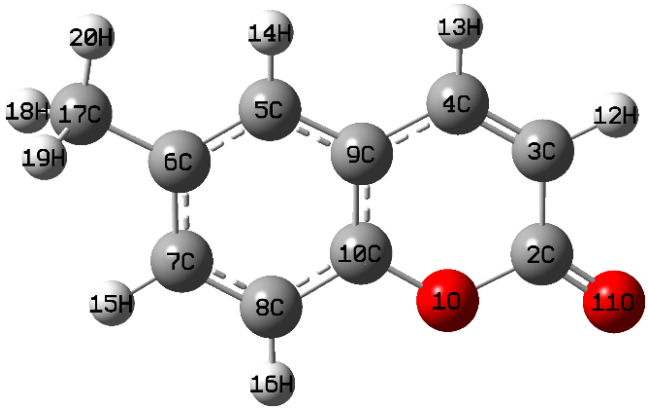

Fig. 1. Optimized geometry and atom numbering of 6-methylcoumarin

TABLE-1
STRUCTURAL PARAMETERS OF
6-METHYLCOUMARIN DETERMINED BY
B3LYP/cc-pVTZ AND B3LYP/6-311++G** METHODS

Structural parameters	B3LYP/cc-pVTZ	B3LYP/6-311++ G**	Expt.[a]
Internuclear distance (Å)			
O1-C2	1.39	1.40	1.372
O1-C10	1.36	1.37	1.384
C2-C3	1.46	1.46	1.472
C2=O11	1.20	1.20	1.208
C3=C4	1.35	1.35	1.341
C3-H12	1.08	1.08	–
C4-C9	1.44	1.44	1.443
C4-H13	1.08	1.09	–
C5-C6	1.39	1.39	1.373
C5-C9	1.40	1.41	1.410
C5-H14	1.08	1.09	–
C6-C7	1.40	1.41	1.414
C6-C17	1.51	1.51	1.529
C7-C8	1.38	1.39	1.376
C7-H15	1.08	1.09	–
C8-C10	1.39	1.39	1.377
C8-H16	1.08	1.08	–
C9-C10	1.40	1.40	1.415
C17-H18	1.09	1.09	–
C17-H19	1.09	1.09	–
C17-H20	1.90	1.09	–
Bond angle (°)			
C2-O1-C10	122.7	122.8	122.4
O1-C2-C3	115.9	115.9	118.0
O1-C2-O11	117.9	117.9	117.7
C3-C2-O11	126.2	126.2	124.3
C2-C3-C4	121.7	121.7	120.1
C3-C4-C9	120.8	120.8	121.1
C6-C5-C9	121.7	121.6	122.7
C5-C6-C7	117.9	118.0	119.6
C5-C6-C17	121.6	121.6	121.2
C7-C6-C17	120.5	120.4	–
C6-C7-C8	121.8	121.8	119.2
C7-C8-C10	119.2	119.1	120.5
C4-C9-C5	124.0	124.0	126.1
C4-C9-C10	117.3	117.3	118.3
C5-C9-C10	118.7	118.7	115.6
O1-C10-C8	117.8	117.7	117.7
O1-C10-C9	121.5	121.5	119.9
C8-C10-C9	120.7	120.8	122.4

[a]Values taken from Ref. [44]

The influence of the substituent on the molecular parameters, particularly in the C-C bond distance of ring carbon atoms is not significant. The mean bond length of aromatic ring is 1.39 Å. More distortion in bond parameters is observed in the hetero ring than in benzene ring. The bond length C2-C3 (1.46 Å) is longer than the other ring C-C bond distances. The C3=C4 and C2=O11 double bond distances were determined as 1.35 Å and 1.20 Å. These are in correlation with 3-acetylcoumarin [15] and 4-hydroxy-1-thiocoumarin [16]. Similarly, the bond length of C6-C17 is 1.51 Å shows the pure single bond nature. The bond length of C9-C10, C4-C9 and C5-C9 are 1.40, 1.44 and 1.40 Å, respectively are well agreed with the literature.

The bond angle decreases when the electronegativity of ligand atoms is more than that of central atom. There is increase in the distance between bond pairs since they are closer to ligand atoms. Due to this, they tend to move closer resulting in the decrease in bond angle. The reduction in bond angles O1-C2-O11 (117º) and O1-C2-C3 (115º) revealed the same. In the case of benzene ring, the electron donating methyl group present at C6 carbon atom significantly influences the bond angle at the point of substitution C5-C6-C9 (117.9º) and is less than 120°. Similarly, the bond angles at the neighbouring atoms C6-C5-C9 (121.7º) and C6-C7-C8 (121.8º) with respect to C6 are more than the normal benzene ring bond angle 120º. The bond angles at the fused ring carbon atoms C9 and C10 are significantly differ because of the hetero nature of the pyrone ring. These are determined as C4-C9-C5 (124º) and O1-C10-C8 (117.8º). The stuructural parameters determined by DFT method are well agreed with the reported coumarin derivatives.

The parameters such as total thermal energy, vibrational energy contribution to the total energy, therotational constants and the dipole moment values obtained from B3LYP method with 6-311++G** and cc-pVTZ basis sets. The energy of the compound 6MC determined by B3LYP/cc-pVTZ method is -536.5327 Hartrees. The total dipole moment of the molecule determined by B3LYP/cc-pVTZ method is 5.32 D.

Analysis of molecular electrostatic potential: The total electron density mapped with electrostatic potential of 6-methylcoumarin constructed by B3LYP/cc-pVTZ method is shown in Fig. 2. The electron density of the molecule lie in the range from $-5.768e \times 10^{-2}$ to $5.768e \times 10^{-2}$. The electrostatic potential spreads between $-4.233e \times 10^{-3}$ and $4.233e \times 10^{-3}$. The colour scheme for the MEP surface is red, electron rich, partially negative charge; blue, electron deficient, partially positive charge; light blue, slightly electron deficient region; yellow, slightly electron rich region; green, neutral; respectively. The region around oxygen atoms represents the most negative potential region (red). The areas around the hydrogen atoms of methyl group and in the ring hydrogen possess the maximum positive charges. The predominance of green region in the ring surfaces corresponds to a potential halfway between the two extremes red and dark blue colour. The total electron density surface mapped with electrostatic potential clearly reveals the presence of high negative charge on the carbonyl oxygen (C=O) while positive charge around the $-CH_3$ group.

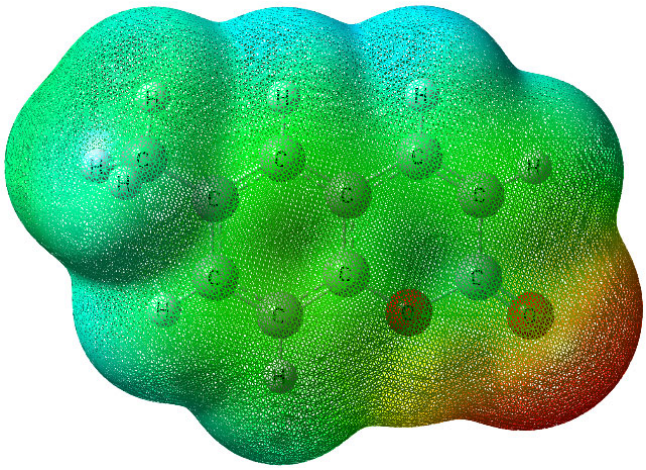

Fig. 2. Total electron density surface mapped with the electrostatic potential of 6-methylcoumarin

Frontier molecular orbitals: The energies of HOMO LUMO, LUMO+1 and HOMO-1 and the LUMO-HOMO orbital energy gap are calculated by using B3LYP/cc-pVTZ method and the pictorial illustration of the frontier molecular orbitals are shown in Fig. 3. The region of HOMO spread over the entire molecule while in the LUMO the ring part has more overlapping. This clearly reveals the possibility of n→π* and π→π* transitions in 6-methylcoumarin. Frontier orbital energy gap ($E_{LUMO} - E_{HOMO}$) of 3-acetylcoumarin [39] and 4-hydroxy-1-thiocoumarin [9] is 4.2085 eV and 4.4115 eV, respectively. The frontier orbital energy gap ($E_{LUMO} - E_{HOMO}$) of 6MC is found to be 4.4831 eV and suggest that 6-methylcoumarin has slightly harder and moderately reactive.

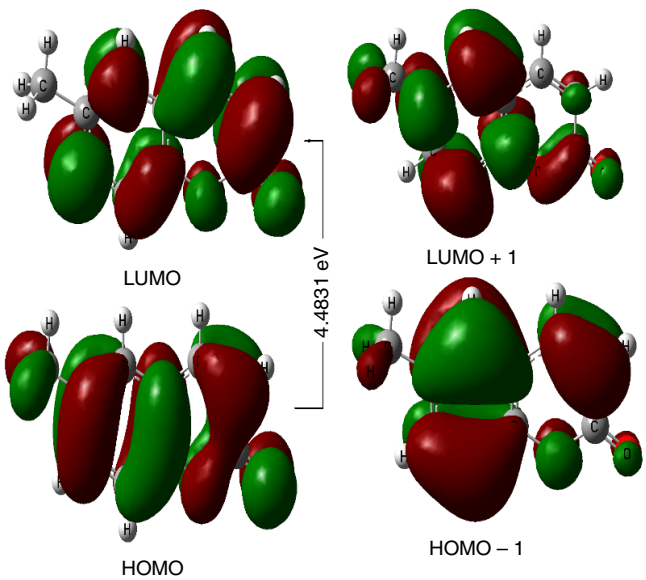

Fig. 3. Frontier molecular orbitals of 6-methylcoumarin

Natural bond orbital (NBO) analysis

Analysis of bonding concepts: The hybridization and delocalization of electron within the molecule has been explained by natural bond orbital analysis (NBO) utilizing B3LYP/cc-pVTZ method. The bonding orbital for C2=O11 with occupancies 1.9801 electrons has 31.02% C2 and 68.98% O11 character. The bonding orbital of C3=C4 with occupancies 1.8287 electrons has 53.53% C3 character and 46.47% C4 character. The presence of double bond in these bonds is confirmed by 100% *p*-character. The bonding orbital for O1-C2 with occupancies 1.9892 electron has 69.04% O1 character in $sp^{2.38}$ hybrid and 30.96 % C2 character in $sp^{2.98}$ hybrid orbital. The bonding orbital for C6-C17 with occupancies 1.9809 electrons has 50.26% C6 character and 49.17% C17 character.

Donor-acceptor interaction energy analysis: The bonding-anti bonding interaction can be quantitatively described in terms of the NBO approach and expressed by means of second-order perturbation interaction energy $E^{(2)}$. The lone pair donor orbital, $n \rightarrow \pi^*$ interaction between the oxygen (O1) lone pair and the C2-O11 and C9-C10 antibonding orbitals are strongly stabilized with 36.29 and 30.06 kcal mol^{-1}, respectively. This reveals the delocalization of oxygen lone pair towards the ring is more probable. The $n_O \rightarrow \sigma^*_{OC}$ stabilization energy of lone pair of electrons presents in the oxygen atom (O11) to the antibonding orbital of O1-C2 is 37.72 kcal mol^{-1}. The bond pair donor orbital, $\pi_{CO} \rightarrow \pi^*_{CC}$ interaction between the C2-O11 bond pair and the C3-C4 antibonding orbital give least stabilization of 5.40 kcal mol^{-1} indicates that it is less likely to occur. The $\pi_{CC} \rightarrow \pi^*_{CC}$ interactions in the aromatic ring possess the stabilization energy in the range 11.01 and 21.83 kcal mol^{-1}.

Vibrational analysis: Using FT-IR and FT-Raman spectra, the vibrational spectral assignments of 6MC have been performed on the basis of reported literature. The accuracy and precision of the vibrational assignments are confirmed by the PED contribution [40] of the respective mode. The observed and theoretically predicted wavenumbers by density functional B3LYP/6-311++G** and B3LYP/cc-pVTZ methods are collected in Table-2. The FT-IR and FT-Raman spectra of 6-methylcoumarin are shown in Figs. 4 and 5, respectively.

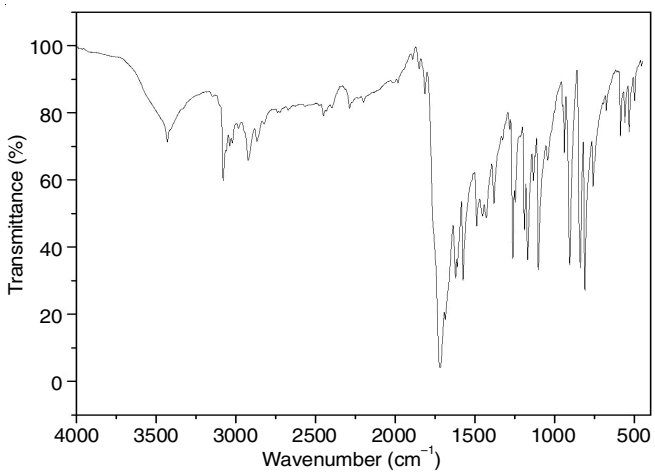

Fig. 4. FT-IR spectrum of 6-methylcoumarin

C-C vibrations: The C-C stretching vibrations are observed in the region 1247-1685 cm^{-1}. Therefore, the fundamental mode observed at 1685 is assigned to the C=C stretching. The other modes 1621, 1575, 1489, 1428, 1326, 1281 and 1261 cm^{-1}

TABLE-2
OBSERVED FT-IR, FT-RAMAN AND CALCULATED FREQUENCIES USING B3LYP/cc-pVTZ AND B3LYP/6-311++G** METHODS ALONG WITH THEIR RELATIVE INTENSITIES AND PROBABLE ASSIGNMENTS OF 6-METHYLCOUMARIN[a]

Observed wavenumber (cm^{-1})		B3LYP/cc-pVTZ calculated wavenumber			B3LYP/6-311++G** calculated wavenumber			Vibration assignment	%PED
FT-IR	FT-Raman	Unscaled (cm^{-1})	Scaled (cm^{-1})	Depolaristion ratio	Unscaled (cm^{-1})	Scaled (cm^{-1})	Depolaristion ratio		
3429 w								2 × 1717	
3079 m	3061 w	3217	3061	0.25	3215	3059	0.23	ν=C-H	$92\nu_{CH}$
3038 w	3040 w	3201	3040	0.23	3200	3038	0.21	νC-H	$87\nu_{CH}$
3021 w	3026 w	3167	3026	0.33	3166	3024	0.24	νC-H	$89\nu_{CH}$
		3166	3039	0.43	3165	3036	0.55	ν=C-H	$90\nu_{CH}$
		3160	3034	0.40	3159	3031	0.37	νC-H	$91\nu_{CH}$
2983 vw	2988 vw	3106	2983	0.75	3105	2981	0.75	ν_aCH_3	$85\nu_{CH3}$
2921 w	2925 w	3074	2921	0.75	3075	2919	0.75	ν_aCH_3	$87\nu_{CH3}$
2867 vw		3028	2867	0.07	3026	2865	0.07	ν_sCH_3	$92\nu_{CH3}$
2286 vw								1169 +1102	
2198 vw								2 × 1102	
1890 vw								2 × 1452	
1717 vs	1716 s	1810	1719	0.34	1801	1716	0.34	νC=O	$95\nu_{C=O}$
1685 vs	1686 vw	1668	1670	0.28	1665	1667	0.26	νC=C	$90\nu_{CC}$
1621 s	1622 m	1654	1624	0.72	1649	1621	0.62	νC-C	$87\nu_{CC}$
1575 s	1576 vs	1604	1578	0.36	1600	1575	0.35	νC-C	$85\nu_{CC}$
1489 m	1492 w	1523	1491	0.25	1517	1488	0.23	νC-C	$89\nu_{CC}$
		1503	1482	0.47	1501	1477	0.44	δ_aCH_3	$87\delta_{CH3} + 12\beta_{CCC}$
1452 m		1487	1455	0.75	1486	1451	0.75	δ_aCH_3	$82\delta_{CH3} + 15\beta_{CCC}$
1428 m		1466	1431	0.75	1461	1427	0.75	νC-C	$82\nu_{CC}$
1381 m	1383 w	1421	1396	0.35	1419	1390	0.37	δ_sCH_3	$80\delta_{CH3} + 16\beta_{CCC}$
		1412	1386	0.21	1405	1382	0.17	νC-C	$81\nu_{CC}$
1326 vw	1326 m	1361	1329	0.25	1361	1325	0.23	νC-C	$87\nu_{CC}$
1281 vw	1280 vw	1304	1283	0.22	1297	1279	0.15	νC-C	$79\nu_{CC}$
1261 s		1287	1264	0.73	1281	1260	0.73	νC-C	$85\nu_{CC}$
1247 m	1248 w	1270	1250	0.22	1266	1246	0.16	$\nu C\text{-}CH_3$	$82\nu_{CC}$
1189 m	1190 vs	1201	1192	0.36	1197	1188	0.37	βC-H	$62\beta_{CH} + 24\beta_{CCC}$
1169 s	1169 vw	1184	1172	0.23	1180	1168	0.19	βC-H	$65\beta_{CH} + 22\beta_{CCC}$
1133 w	1126 vw	1154	1136	0.16	1149	1132	0.14	βC-H	$67\beta_{CH} + 18\beta_{CCC}$
1102 s	1103 vw	1101	1105	0.26	1093	1101	0.30	νC-O	$79\nu_{CO}$
1043 w		1069	1046	0.75	1063	1042	0.74	ωCH_3	$62\omega_{CH3} + 25\gamma_{CCC}$
		1025	1008	0.50	1022	1001	0.53	τCH_3	$59\tau_{CH3} + 28\gamma_{CCC}$
	989 vw	1023	992	0.75	1004	988	0.75	β=C-H	$60\beta_{CH} + 24\beta_{CCC}$
		983	966	0.75	969	949	0.75	β=C-H	$62\beta_{CH} + 19\beta_{CCC}$
939 w	946 w	962	949	0.14	957	945	0.13	βCCC	$59\beta_{CCC} + 26\beta_{CH}$
905 s	906 vw	911	908	0.36	906	904	0.42	νC-O	$83\nu_{CO}$
		910	895	0.75	896	877	0.75	γC-H	$59\gamma_{CH} + 21\gamma_{CCC}$
838 s	847 vw	856	842	0.30	852	837	0.33	βCOC	$67\beta_{COC} + 19\beta_{C=O}$
		853	840	0.75	839	821	0.75	γ=C-H	$62\gamma_{CH} + 18\gamma_{CCC}$
811 s		847	815	0.75	835	810	0.75	γ=C-H	$60\gamma_{CH} + 25\gamma_{CCC}$
759 m	758 m	783	763	0.75	762	758	0.06	γC-H	$59\gamma_{CH} + 24\gamma_{CCC}$
		765	754	0.08	759	743	0.75	βCCC	$54\beta_{CCC} + 21\beta_{CH}$
	692 vw	707	696	0.75	694	691	0.75	γC-H	$56\gamma_{CH} + 24\gamma_{CCC}$
676 vw	676 vw	687	680	0.38	685	675	0.42	βCCC	$58\beta_{CCC} + 22\beta_{CH}$
587 w	586 vw	591	593	0.68	589	588	0.75	βCCO	$56\beta_{CCO} + 20\beta_{CH}$
559 w		576	563	0.75	562	558	0.75	βCCC	$57\beta_{CCC} + 23\beta_{CH}$
532 w	534 w	544	536	0.72	542	531	0.73	βOCC	$58\beta_{CCO} + 25\beta_{C=O}$
498 w	500 w	505	502	0.37	502	497	0.36	βC=O	$62\beta_{C=O} + 24\beta_{CCO}$
450 vw	453 vw	470	457	0.75	461	452	0.75	γCCC	$55\gamma_{CCC} + 26\gamma_{CH}$
	423 m	422	427	0.24	421	422	0.21	γCCC	$56\gamma_{CCC} + 21\gamma_{CH}$
	374 w	385	378	0.75	379	373	0.75	γCCC	$54\gamma_{CCC} + 22\gamma_{CH}$
	362 w	364	366	0.42	363	361	0.40	$\beta C\text{-}CH_3$	$59\beta_{CC} + 18\beta_{CH}$
	247 vw	345	252	0.75	336	246	0.75	γCOC	$62\gamma_{COC} + 21\gamma_{C=O}$
	202 vw	240	207	0.29	240	201	0.31	γCCO	$54\gamma_{CCO} + 23\gamma_{CH}$
	183 w	179	188	0.75	173	182	0.75	$\gamma C\text{-}CH_3$	$52\gamma_{CC} + 20\gamma_{CH}$
		161	163	0.75	156	152	0.75	γCCC	$54\gamma_{CCC} + 21\gamma_{CH}$
		80	83	0.75	78	75	0.75	γCCC	$57\gamma_{CCC} + 22\gamma_{CH}$
		46	50	0.75	49	47	0.75	γCCC	$52\gamma_{CCC} + 24\gamma_{CH}$

[a]ν-stretching; β-in-plane bending; δ-deformation; ρ-rocking; γ-out of plane bending; ω-wagging and τ-twisting.

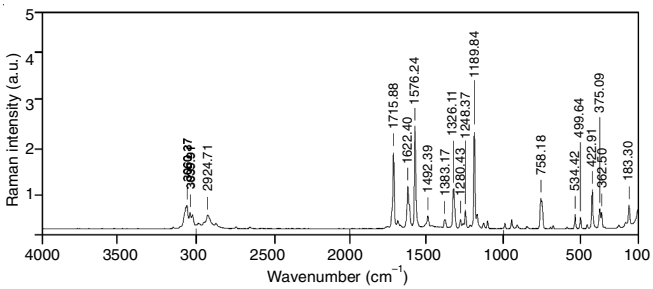

Fig. 5. FT-Raman spectrum of 6-methylcoumarin

observed in the infrared spectrum are attributed to the carbon-carbon stretching vibrations of the ring. The fundamental mode observed at 1247 cm^{-1} is assigned to C-CH_3 stretching vibration. All CCC in-plane bending and CCC out of plane bending modes are observed in the region below 1000 cm^{-1} [39,41]. The bands corresponding to COC, CCO and OCC in-plane bending vibrations are assigned at 838, 587 and 532 cm^{-1}, respectively in infrared spectrum whereas in the Raman spectrum these are attributed to 847 and 586 cm^{-1}, respectively. The CCC in-plane bending modes are assigned to 939, 676 and 559 cm^{-1} mode in IR spectrum. The modes observed in the Raman spectrum at 453, 423 and 374 cm^{-1} are assigned to CCC out of plane bending vibrations.

C-H vibrations: The C-H stretching vibrations of benzene derivatives generally appear in the region of 3000-3100 cm^{-1} [9,39,42]. In this region, the aromatic C-H stretching bands are found to be weak and this is due to a decrease of the dipole moment caused by the reduction of negative charge on the carbon atom. This reduction occurs because of the electron withdrawal on the carbon atom by the substituent due to the decrease of inductive effect, which in turn is caused by the increase in chain length of the substituent [43]. Hence, the bands obtained at 3038, 3021 cm^{-1} in IR and 3040, 3026 cm^{-1} in Raman spectrum are assigned to C-H stretching vibrations. The bands appeared at 1189, 1169, 1133 cm^{-1} in infrared and at 1190, 1169 and 1126 in Raman spectra are assigned to the aromatic C-H in-plane bending vibrations. The aromatic C-H out of plane bending vibrations are observed in Raman at 758 and 692 cm^{-1}. The alkenyl =C-H stretching appears in the higher end at 3079 and 3061 cm^{-1} in IR and Raman spectra, respectively. Another =C-H vibration is determined by DFT at 3039 cm^{-1}. The separation between these two modes is due to in-phase and out of phase in nature. The strong band obtained in IR at 811 is assigned to =C-H out of plane bending mode.

Methyl group vibrations: The asymmetric and symmetric stretching modes of -CH_3 group normally appear below 3000 cm^{-1} [44,45]. The bands observed at 2983, 2921 and 2988, 2925 cm^{-1} in IR and Raman spectra, respectively are fully depolarized and assigned as asymmetric stretching vibrations of -CH_3 group. The symmetric methyl stretching is assigned to 2687 cm^{-1}. This assignment is in good agreement to the asymmetric stretching frequency for -CH_3 group observed in 3-methylcoumarin at 2900 cm^{-1} [12]. The -CH_3 deformations are expected in the region 1370-1465 cm^{-1}. So, the medium IR band observed at 1452 cm^{-1} is assigned to asymmetric deformation of -CH_3 group. The symmetric methyl deformation is attributed to the medium band at 1381 cm^{-1}. All other related fundamentals of methyl group are listed in Table-2.

C=O and C-O vibrations: Almost all carbonyl compounds have a very intense and narrow peak in the range of 1800-1600 cm^{-1} [45,46]. Coumarins have two characteristic strong absorption bands arising from C=O and C-O stretching vibrations. The intense C=O stretching vibration of coumarin occurs at higher frequencies than that of normal ketones. In case of 3-(bromoacetyl)coumarin, the C=O stretching vibration observed at 1747 cm^{-1} and C-O stretching vibrations observed at 1216 cm^{-1} [47]. Udaya Sri & Chaitanya [48] observed the strong band in FT-IR spectrum at 1720 cm^{-1} and a weak band in FT-Raman spectrum at 1741 cm^{-1} and assigned to the C=O stretching vibration [18]. In 6-methylcoumarin, the very strong band observed at 1717 cm^{-1} in FT-IR and the strong band at 1716 cm^{-1} in FT-Raman spectrum are readily assigned to the C=O vibration. In the present investigation, the overtone for C=O group is observed at 3429 cm^{-1} as weak band, confirmed the assignment of C=O stretching vibration. The C-O stretching vibration is observed at 1102/1103 and 905/906 cm^{-1} in FT-IR/FT-Raman spectra of 6-methylcoumarin.

Scale factors: The inclusion of anhormonicity in the computed frequencies can be eliminated by scaling the theoretical wavenumbers. The linear scaling equation method has been used to brings the experimental and theoretical vibrational frequencies closer together [49-52]. The scaling equation $y = 0.9996x - 0.5999$ and $y = 0.9983x + 5.0087$ were used in the case of 6-methylcoumarin with 6-311++G** and cc-pVTZ basis sets, respectively.

NMR spectral studies: The ^{13}C and ^{1}H NMR chemical shifts have been determined with B3LYP/cc-pVTZ method using the gauge independent atomic orbital (GIAO) method [34,35]. The ^{1}H and ^{13}C theoretical and experimental chemical shifts, isotropic shielding constants and the assignments of 6-methylcoumarin are presented in Table-3. The observed ^{1}H and ^{13}C NMR spectra of 6-methylcoumarin in $CDCl_3$ solvent is given in the Figs. 6 and 7, respectively.

The hyperconjugative effect of methyl group is most pronounced on the chemical shifts of the protons H18, H19 and H20. Hence these are all give a singlet in the highly shielded position with chemical shift of 2.38 ppm. The singlet peak observed at 7.25 ppm is assigned to H14. All other hydrogen atoms produce doublet signals. The H13 is highly deshielded at 7.64 ppm. The deshielded proton H16 and H12 shows the doublet signals at 7.30 and 7.31 ppm, respectively. The calculated and experimental chemical shift values show very good agreement with each other.

Unsaturated carbons give signals in the region 100-200 ppm [53]. The highly deshielded carbon C2 appears at 161.02 ppm. The more chemical shift of C4 (152.13 ppm) indicate the direction of delocalization of electrons towards the carbonyl carbon. Among the ring carbon atoms C10 is highly shielded signifies that lone pair of O1 move towards the ring. All other aromatic carbon atoms have the chemical shift in the range 116.48-143.45 ppm. Comparing the chemical shift positions of ring carbon atom with that of methyl carbon atom (C17), the upfield chemical shift of methyl carbon (20.67 ppm) is

TABLE-3
EXPERIMENTAL AND THEORETICAL ^{1}H AND ^{13}C NMR CHEMICAL SHIFTS (δ_{iso}, ppm) WITH RESPECT TO TMS AND SHIELDING CONSTANTS (σ_{iso}) OF 6-METHYLCOUMARIN

Atom	Shielding constant (σ_{iso})	Isotropic chemical shift (δ_{iso}, ppm)	Expt.
C2	18.55	165.98	161.02
C3	64.34	120.19	116.48
C4	33.27	151.27	152.13
C5	50.73	133.81	132.80
C6	42.85	141.68	143.45
C7	45.38	139.15	134.13
C8	63.12	121.41	118.56
C9	59.55	124.99	127.71
C10	22.90	161.64	77.14
H12	25.36	6.61	7.31
H13	23.77	8.20	7.64
H14	24.20	7.77	7.25
H15	24.00	7.97	7.18
H16	24.27	7.70	7.30
C17	162.02	22.52	20.67
H18	29.10	2.87	2.38
H19	29.10	2.87	2.38
H20	29.55	2.43	2.38

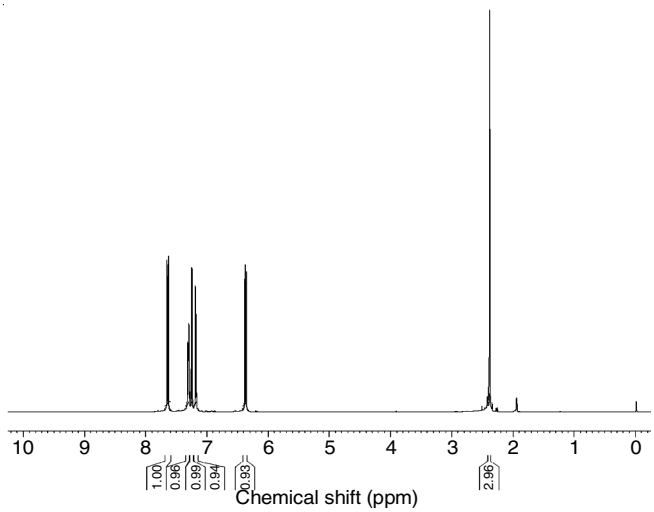

Fig. 6. ^{1}H NMR spectrum of 6-methylcoumarin

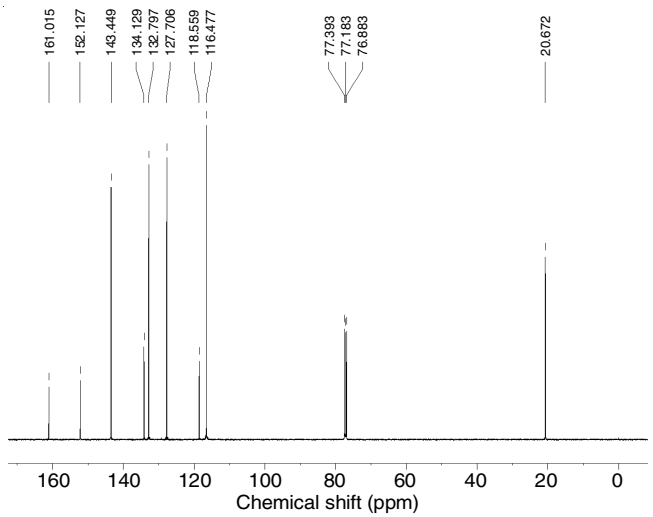

Fig. 7. ^{13}C NMR spectrum of 6-methylcoumarin

due to the hyperconjugative effect of methyl group. The triplet peak obtained at around 77 ppm is due the $CDCl_3$ solvent.

Analysis of a structure-activity relations

Atomic charge distribution: The atomic charges of neutral, cationic and anionic species of 6-methylcoumarin calculated by NBO analysis with B3LYP/cc-pVTZ method. Among the carbon atoms C2 and C10 has positive charge while others have negative charge. The positive charge of C4 is due to the attachment of highly electronegative oxygen atom (O1) to it. The more positive charge on C2 and highly negative O11 indicates the polar nature of the carbonyl group. The electron donating nature of methyl group by means of hyperconjugative effect makes the carbon atom C17 with high negative charge.

Reactivity properties: The global parameters ionization potential (I), electron affinity (A), electrophilicity (ω), electronegativity (χ), hardness (η) and softness (S) of the molecule were determined. The local reactivity data revealed that the nucleophilic attack is favourable at C9 and C17. The order of electrophilic attack is C17 > C2 > C5. The methyl carbon may be replaced by any other groups by electrophilic, nucleophilic or free radical attack. From the dual reactivity descriptors, the atoms C6, C9 and C10 are favourable for nucleophilic attack. The other atoms are more prone to electrophilic attack. This indicates the possibility of the breaking of C9-C4 and C10-O1 bonds to produce benzene derivatives.

Conclusion

The geometry of 6-methylcoumarin under investigation was optimized by B3LYP method using cc-pVTZ and 6-311++G** basis sets. The vibrational frequencies were assigned, elaborated in detail and compared with the theoretical frequencies. The chemical reactivity and site selectivity of the molecule has been determined with the help of global and local reactivity descriptors. The kinetic stability has been examined by LUMO-HOMO energy gap. The carbon and hydrogen environment have been investigated in detailed manner utilizing NMR spectroscopy. Thus, the present investigation provides geometrical parameters, kinetic and thermodynamic stability of the molecule, chemical reactivity, the energy gap between the frontier molecular orbitals, the probable electronic transitions and chemical shifts of the compound.

CONFLICT OF INTEREST

The authors declare that there is no conflict of interests regarding the publication of this article.

REFERENCES

1. C.S. Francisco, C.S. Francisco, A.F. Constantino, Á.C. Neto and V. Lacerda Jr., *Curr. Org. Chem.*, **23**, 2722 (2019); https://doi.org/10.2174/1385272823666191121150047
2. F. Annunziata, C. Pinna, S. Dallavalle, L. Tamborini and A. Pinto, *Int. J. Mol. Sci.*, **21**, 4618 (2020); https://doi.org/10.3390/ijms21134618
3. A. Stefanachi, F. Leonetti, L. Pisani, M. Catto and A. Carotti, *Molecules*, **23**, 250 (2018); https://doi.org/10.3390/molecules23020250
4. L.C. Di Stasi, *Molecules*, **26**, 422 (2021); https://doi.org/10.3390/molecules26020422

5. C.T. Supuran, *J. Enzym. Inhibit. Med. Chem.*, **35**, 1462 (2020); https://doi.org/10.1080/14756366.2020.1788009
6. A. Bouhaoui, M. Eddahmi, M. Dib, M. Khouili, A. Aires, M. Catto and L. Bouissane, *ChemistrySelect*, **6**, 5848 (2021); https://doi.org/10.1002/slct.202101346
7. K.N. Venugopala, Rashmi and B. Odhav, *BioMed Res. Int.*, **2013**, 963248 (2013); https://doi.org/10.1155/2013/963248
8. H. Chang, M. Shi, Y.-N. Sun and J.-Q. Jiang, *Chin. J. Polym. Sci.*, **33**, 1086 (2015); https://doi.org/10.1007/s10118-015-1657-4
9. V. Arjunan, S. Sakiladevi, M.K. Marchewka and S. Mohan, *Spectrochim. Acta A Mol. Biomol. Spectrosc.*, **109**, 79 (2013); https://doi.org/10.1016/j.saa.2013.01.100
10. V. Arjunan, R. Santhanam, S. Sakiladevi, M.K. Marchewka and S. Mohan, *J. Mol. Struct.*, **1037**, 305 (2013); https://doi.org/10.1016/j.molstruc.2013.01.014
11. A. Stamm, K. Schwing and M. Gerhards, *J. Chem. Phys.*, **141**, 194304 (2014); https://doi.org/10.1063/1.4900893
12. M. Arivazhagan, R. Kavitha and V.P. Subhasini, *Spectrochim. Acta A Mol. Biomol. Spectrosc.*, **130**, 502 (2014); https://doi.org/10.1016/j.saa.2014.04.001
13. N. Udaya Sri, K. Chaitanya, M.V.S. Prasad, V. Veeraiah and A. Veeraiah, *Spectrochim. Acta A Mol. Biomol. Spectrosc.*, **97**, 728 (2012); https://doi.org/10.1016/j.saa.2012.07.055
14. J. Tonannavar, J. Yenagi, V. Sortur, V.B. Jadhav and M.V. Kulkarni, *Spectrochim. Acta A Mol. Biomol. Spectrosc.*, **77**, 351 (2010); https://doi.org/10.1016/j.saa.2010.03.013
15. A. Ramoji, J. Yenagi, J. Tonannavar, V.B. Jadhav and M.V. Kulkarni, *Spectrochim. Acta A Mol. Biomol. Spectrosc.*, **77**, 1039 (2010); https://doi.org/10.1016/j.saa.2010.08.070
16. I. Sidir, Y.G. Sidir, M. Kumalar and E. Tasal, *J. Mol. Struct.*, **964**, 134 (2010); https://doi.org/10.1016/j.molstruc.2009.11.023
17. A.N. Castro, L.R. Almeida, M.M. Anjos, G.R. Oliveira, H.B. Napolitano, C. Valverde and B. Baseia, *Chem. Phys. Lett.*, **653**, 122 (2016); https://doi.org/10.1016/j.cplett.2016.04.070
18. F. Zhang, H. Zhang, D. Fang and Q. Liu, *Spectrochim. Acta A Mol. Biomol. Spectrosc.*, **71**, 710 (2008); https://doi.org/10.1016/j.saa.2008.01.035
19. V. Sortur, J. Yenagi, J. Tonannavar, V.B. Jadhav and M.V. Kulkarni, *Spectrochim. Acta A Mol. Biomol. Spectrosc.*, **64**, 301 (2006); https://doi.org/10.1016/j.saa.2005.07.024
20. R.O. Juvonen, M. Kuusisto, C. Fohrgrup, M.H. Pitkanen, T.J. Nevalainen, S. Auriola, H. Raunio, M. Pasanen and O.T. Pentikainen, *Xenobiotica*, **46**, 14 (2015); https://doi.org/10.3109/00498254.2015.1048327
21. A.R. Hernández, L.F. Ospina and D.M. Aragón, *Biomed. Chromatogr.*, **29**, 176 (2015); https://doi.org/10.1002/bmc.3253
22. J.-S. Lan, L.-F. Pan, S.-S. Xie, X.-B. Wang and L.-Y. Kong, *Med. Chem. Commun.*, **6**, 592 (2015); https://doi.org/10.1039/C4MD00437J
23. M.J. Matos, F. Pérez-Cruz, S. Vazquez-Rodriguez, E. Uriarte, L. Santana, F. Borges and C. Olea-Azar, *Bioorg. Med. Chem.*, **21**, 3900 (2013); https://doi.org/10.1016/j.bmc.2013.04.015
24. B.C. Pemberton, A. Ugrinov and J. Sivaguru, *J. Photochem. Photobiol. Chem.*, **255**, 10 (2013); https://doi.org/10.1016/j.jphotochem.2013.01.005
25. J.-F. Nie, H.-L. Wu, S.-H. Zhu, Q.-J. Han, H.-Y. Fu, S.-F. Li and R.-Q. Yu, *Talanta*, **75**, 1260 (2008); https://doi.org/10.1016/j.talanta.2008.01.026
26. P. Hohenberg and W. Kohn, *Phys. Rev. B*, **136(3B)**, 864 (1964); https://doi.org/10.1103/PhysRev.136.B864
27. A.D. Becke, *J. Chem. Phys.*, **98**, 5648 (1993); https://doi.org/10.1063/1.464913
28. A.D. Becke, *Phys. Rev. A*, **38**, 3098 (1988); https://doi.org/10.1103/PhysRevA.38.3098
29. C. Lee, W. Yang and R.G. Parr, *Phys. Rev. B Condens. Matter*, **37**, 785 (1988); https://doi.org/10.1103/PhysRevB.37.785
30. M.J. Frisch, G.W. Trucks, H.B. Schlegel, G.E. Scuseria, M.A. Robb, J.R. Cheeseman, G. Scalmani, V. Barone, B. Mennucci, G.A. Petersson, H. Nakatsuji, M. Caricato, X. Li, H.P. Hratchian, A.F. Izmaylov, J. Bloino, G. Zheng, J.L. Sonnenberg, M. Hada, M. Ehara, K. Toyota, R. Fukuda, J. Hasegawa, M. Ishida, T. Nakajima, Y. Honda, O. Kitao, H. Nakai, T. Vreven, J.A. Montgomery Jr., J.E. Peralta, F. Ogliaro, M. Bearpark, J.J. Heyd, E. Brothers, K.N. Kudin, V.N. Staroverov, R. Kobayashi, J. Normand, K. Raghavachari, A. Rendell, J.C. Burant, S.S. Iyengar, J. Tomasi, M. Cossi, N. Rega, J.M. Millam, M. Klene, J.E. Knox, J.B. Cross, V. Bakken, C. Adamo, J. Jaramillo, R. Gomperts, R.E. Stratmann, O. Yazyev, A.J. Austin, R. Cammi, C. Pomelli, J.W. Ochterski, R.L. Martin, K. Morokuma, V.G. Zakrzewski, G.A. Voth, P. Salvador, J.J. Dannenberg, S. Dapprich, A.D. Daniels, O. Farkas, J.B. Foresman, J.V. Ortiz, J. Cioslowski and D.J. Fox, Gaussian, Inc., Wallingford, CT (2009).
31. J.S. Murray and K. Sen, Molecular Electrostatic Potentials, Concepts and Applications, Elsevier, Amsterdam (1996).
32. R.I. Dennington, T. Keith and J. Millam, GaussView, Version 5.0.8, Semichem. Inc., Shawnee Mission, KS (2008).
33. J.P. Foster and F. Weinhold, *J. Am. Chem. Soc.*, **102**, 7211 (1980); https://doi.org/10.1021/ja00544a007
34. A.E. Reed, R.B. Weinstock and F. Weinhold, *J. Chem. Phys.*, **83**, 735 (1985); https://doi.org/10.1063/1.449486
35. A.E. Reed and F. Weinhold, *J. Chem. Phys.*, **78**, 4066 (1983); https://doi.org/10.1063/1.445134
36. R. Ditchfield, *J. Chem. Phys.*, **56**, 5688 (1972); https://doi.org/10.1063/1.1677088
37. K. Wolinski, J.F. Hinton and P. Pulay, *J. Am. Chem. Soc.*, **112**, 8251 (1990); https://doi.org/10.1021/ja00179a005
38. M.K. Kokila, A. Jain, Puttaraja, M.V. Kulkarni and N.C. Shivaprakash, *Acta Crystallogr. C*, **51**, 2585 (1995); https://doi.org/10.1107/S0108270195006263
39. Y. Yamada, M. Okamoto, H. Kikuzaki and N. Nakatani, *Biosci. Biotechnol. Biochem.*, **61**, 740 (1997); https://doi.org/10.1271/bbb.61.740
40. H. Fuhrer, V.B. Kartha, K.L. Kidd, P.J. Kruger and H.H. Mantsch, Computer Program for Infrared and Spectrometry, Normal Coordinate Analysis, National Research Council, Ottawa, Canada, vol. 5 (1976).
41. Y. Uesugi, M. Mizuno, A. Shimojima and H. Takahashi, *J. Phys. Chem. A*, **101**, 268 (1997); https://doi.org/10.1021/jp9626881
42. V. Krishnakumar and R.J. Xavier and *J. Indian Pure Appl. Phys.*, **41**, 597 (2003).
43. M.K. Subramanian, P.M. Anbarasan and S. Manimegalai, *Pramana- J. Phys.*, **74**, 845 (2010); https://doi.org/10.1007/s12043-010-0104-x
44. B.C. Smith, Infrared Spectral Interpretation: A Systematic Approach, CRC Press, Boca Raton, Florida (1998).
45. G. Socrates, Infrared and Raman Characteristic Group Frequencies – Tables and Charts, John Wiley & Sons, Chichester, Ed.: 3 (2001).
46. G. Varsanyi, Vibrational Spectra of Benzene Derivatives, Academic Press: NewYork (1969).
47. N.P. Roeges, A Guide to the Complete Interpretation of Infrared Spectra of Organic Structures, Wiley: New York (1994).
48. N. Udaya Sri, K. Chaitanya, M.V.S. Prasad, V. Veeraiah and A. Veeraiah, *Spectrochim. Acta A Mol. Biomol. Spectrosc.*, **97**, 728 (2012); https://doi.org/10.1016/j.saa.2012.07.055
49. V. Arjunan and S. Mohan, *J. Mol. Struct.*, **892**, 289 (2008); https://doi.org/10.1016/j.molstruc.2008.05.053
50. V. Arjunan and S. Mohan, *Spectrochim. Acta A Mol. Biomol. Spectrosc.*, **72**, 436 (2009); https://doi.org/10.1016/j.saa.2008.10.017
51. J.O. Jensen, A. Banerjee, C.N. Merrow, D. Zeroka and J. Michael Lochner, *J. Mol. Struct. THEOCHEM*, **531**, 323 (2000); https://doi.org/10.1016/S0166-1280(00)00465-6
52. V. Arjunan, P. Ravindran, T. Rani and S. Mohan, *J. Mol. Struct.*, **988**, 91 (2011); https://doi.org/10.1016/j.molstruc.2010.12.032
53. R.M. Silverstein, G.C. Bassler and T.C. Morrill, Spectrometric Identification of Organic Compounds, Wiley: New York, Ed.: 5, p. 245 (1991).